Journal of Ceramic Processing Research. Vol. 18, No. 4, pp. 291~300 (2017)

J O U R N A L O F
Ceramic Processing Research

Study on the pozzolanic activity of finely ground bottom ash for cement replacement

Jeong-Bae Lee[a,*], Seong-Soo Kim[a], Jin-Yong Lee[b] and Jae-Suk Ryou[c]

[a]Department of Civil Engineering, Daejin University, 1007 Hoguk-ro, Pocheon-si, Gyeonggi-Do 11159, Republic of Korea
[b]KMB. CO., Ltd, #46, 3-Gil, 2-Gongdan, Miyang-Myon, Ansung-Si, Gyeonggi-Do, Republic of Korea
[c]Department of Civil & Environmental Engineering, Hanyang University, 17 Haengdang-dong, Seongdong-gu, Seoul 04763, Korea

This study experimentally investigated the properties of bottom ash in cement specimens. The performances of hardened cement test specimens, prepared with unground or finely ground bottom ash, fly ash, or ordinary Portland cement, were compared. The fineness of bottom ash increased with grinding time. Testing in mortar mixes revealed that the compressive strengths of both wet and dry finely ground bottom ash increased with increasing fineness. The microstructural density of bottom ash increased and the porosity decreased as the grinding fineness increased. Finely ground bottom ash showed strong pozzolanic activity, demonstrating its applicability as a cement replacement.

Key words: Bottom ash, Pozzolanic reaction, Waste materials, Filler, Particle size.

Introduction

With the steady increase in global power consumption, the number of power plants increases constantly worldwide. Despite the recent increased interest in researching and constructing facilities for green power generation from renewable sources, such as wind and solar energy, these cannot meet the demand for electricity. In South Korea, the majority of power generation facilities are nuclear and thermal power plants. However, general aversion to nuclear power has increased since the Fukushima nuclear power plant explosion in March 2011, caused by the earthquake that struck the northeastern region of Japan; no suitable alternatives to nuclear energy exist other than thermal power plants.

As of 2015, 66% of the total global electricity output was generated in thermal power plants, of which 42.8% was from coal-fired power plants. The abundance of coal reserves and the high efficiency of facility investment guarantee coal to be the most important energy source for power generation for the next 300-400 years. With the increasing output of thermal power plants, the production of coal ash as waste is steadily increasing, from 8 million tons in 2012 to 9 million tons expected in 2015.

Coal ash is divided into fly ash and bottom ash based on the discharge height in the boiler where it is formed. Fly ash, 80% by weight of the total coal ash generated, has long been recycled as a representative partial replacement material for Portland cement, e.g., as concrete admixture, because it has spherical particle shapes. Bottom ash, 10-15% of coal ash, has a higher proportion of unburned carbon and consists of irregularly shaped porous particles, characterized by high water absorption and low abrasion resistance. Therefore, unlike the highly recyclable fly ash, bottom ash is not easily recycled and has very limited applications as a lightweight aggregate, aggregate in road bases and sub-bases, and floor filling material. The reuse potential of bottom ash is limited because few empirical studies or quality standards exist for the material; most bottom ash is buried in coastal landfills local to power plants. Therefore, a pressing need exists for research on bottom ash reuse, to solve the problems associated with landfill site selection and environmental contamination.

Some studies have attempted to use bottom ash as a replacement of aggregates, using the morphological similarity of the ash to common aggregates. Topçu and Bilir [1] studied the effects of bottom ash addition on the cracking and contraction of concrete in experiments with mortars containing bottom ash as fine aggregates. They reported that the optimal values were obtained at replacement ratios of 40-50% in tests of compressive strength and ultrasonic pulse velocity, with higher bottom ash contents promoting proportionally lower crack generation and smaller crack sizes.

Yüksel and Genç [2] compared the performances of concrete specimens using fine aggregates of blast furnace slag and bottom ash, and reported that the replacement with bottom ash and blast furnace slag reduced the compressive strength. The reduction was greater with bottom ash than with blast furnace slag; they set the upper limit for the replacement ratio to 10% to satisfy the maximum 10% decrease in the compressive strength of concrete.

*Corresponding author:
Tel : +82-31-531-4432
Fax: +82-31-533-9580
E-mail: dlwjdqo@nate.com

Singh and Siddique [3] studied the properties of concrete containing low-calcium bottom ash as fine aggregates. According to the reported results, the adverse effect on compressive strength was negligible at a replacement ratio of 50%, and the compressive strength was improved from Day 28 onward because of the pozzolanic reaction of bottom ash, verified by microstructural analysis. The feasibility of using bottom ash as a fine aggregate was also tested by analyzing the effects of the material on the chloride penetration resistance and chemical attack resistance of the concrete. The results were consistent with those of a study conducted by Ghafoori and Buchole [4], which showed that bottom ash in aggregates increased the water content for increasing flow volumes because of the porosity and angular surface morphology of the ash particles. This caused an initial decrease in the strength because of the high water content, but the strength was recovered as the age increased to a level nearly matching that of the reference concrete. They also reported that the addition of a superplasticizer improved the strength and bleeding, demonstrating a considerable performance enhancement.

Another recycling potential for bottom ash is cement replacement. Kula et al. [5] compared the performances of cement pastes with bottom ash and fly ash partially replacing cement, and reported that the cement paste containing bottom ash showed a reduced compressive strength at early ages but a higher strength than that of the pure cement paste by Day 28.

Cheriaf et al. [6] studied the effects of bottom ash on the consumption of calcium hydroxide ($Ca(OH)_2$) and the pozzolanic activity as a function of the bottom ash grinding time, reporting that the ash reacted slowly with $Ca(OH)_2$ in early ages but began reacting more intensively on Day 28, reaching a peak on Day 91. Longer grinding times for the bottom ash corresponded to higher compressive strengths.

This study was conducted to investigate the feasibility of bottom ash as cement replacement, focusing on the pozzolanic reaction of the material. To induce more intense pozzolanic reactions, the bottom ash was ground with a ball mill. Test specimens were prepared with two types of bottom ash, depending on the cooling method, and the bottom ash particles were ground to four fineness levels.

Material and Methods

Two types of bottom ash were selected for testing: dry and wet types, depending on the discharge method. The bottom ash was finely ground to change the porosity and morphology and to increase the pozzolanic activity. Finely ground particles of bottom ash were obtained with four different degrees of grinding fineness by varying the grinding time in the ball mill as 1, 2, 4, and 8 hrs.

Table 1. Chemical composition and physical properties of ordinary Portland cement.

Chemical composition (%)		Physical properties		
SiO_2	21.7	Density (g/cm^3)		3.12
Al_2O_3	5.7	Fineness(cm^2/g)		3 490
Fe_2O_3	3.2	Sat. time (min)	Initial set.	264
CaO	63.1		Final set.	317
MgO	2.8	Compressive strength (Mpa)	3 days	30.0
SO_3	2.2		7 days	43.6
Ignition loss	1.3		28 days	55.1

Table 2. Chemical composition and physical properties of fly ash and bottom ash. (The Samcheonpo Coal Power Plant).

Chemical composition (%)	Fly ash	Bottom ash (Type 1)	Bottom ash (Type 2)
SiO_2	58.06	52.0	51.43
Al_2O_3	18.16	23.5	23.23
Fe_2O_3	8.11	9.63	6.91
CaO	3.54	8.09	3.24
MgO	1.25	1.89	0.77
TiO_2	0.93	1.36	1.29l
Na_2O	0.38	0.59	0.4
Ignition loss	2.2	–	–

Table 3. Physical properties of fly ash and bottom ash.

Section	Fly ash	Bottom ash (Type 1)	Bottom ash (Type 2)
Density (g/cm^3)	2.29	1.86	2.16
Fineness (cm^2/g)	423	–	–
Ignition loss(%)	–	1.7	12.0

Table 4. Physical properties of river sand excavated from Jumunjin beach.

Density (g/cm^3)	Absorption (%)	Fineness modulus
2.63	0.48	2.92

Table 5. Mean particle size of bottom ash depending on grinding time and fineness.

Bottom ash Type \ Grin-ding time		1 hr	2 hr	4 hr	8 hr
Type 1	Fineness (cm^2/g)	115	224	347	643
	Mean particle size (μm)	114	33.8	31.7	12.4
	Ignition loss (%)	1.76	1.70	1.89	2.10
Type 2	Fineness (cm^2/g)	325	549	600	902
	Mean particle size (μm)	34.6	15.9	14.8	12.2
	Ignition Loss (%)	10.94	10.61	11.25	11.97

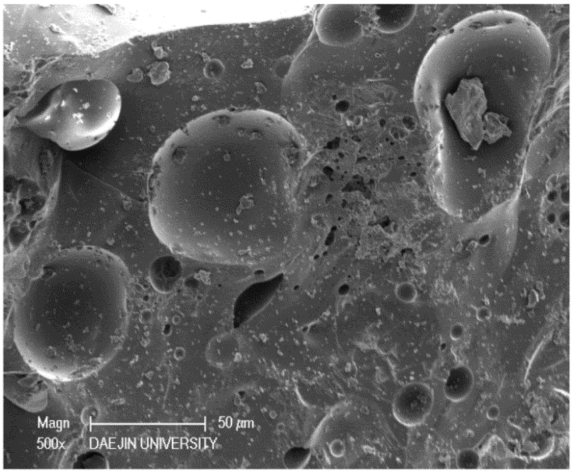

Fig. 1. Pre-grinding bottom ash (Type 1) (× 500).

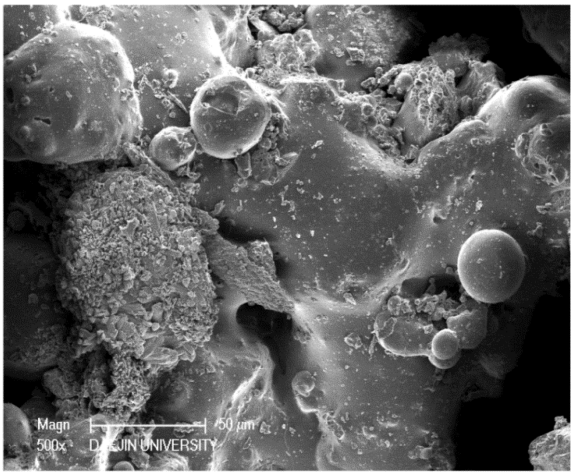

Fig. 2. Pre-grinding wet bottom ash (Type 2) (× 500).

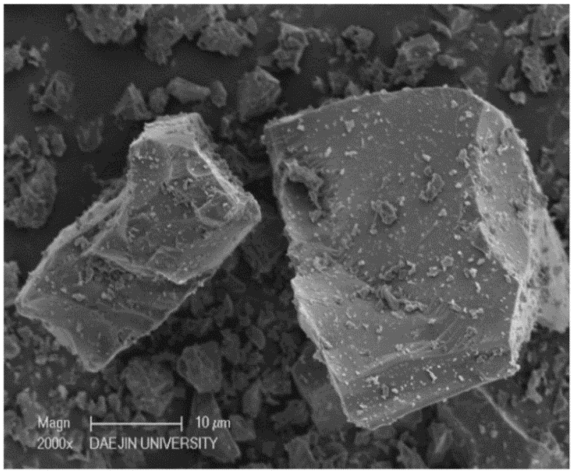

Fig. 3. 2 hrs ground bottom ash (Type 1) (× 2,000).

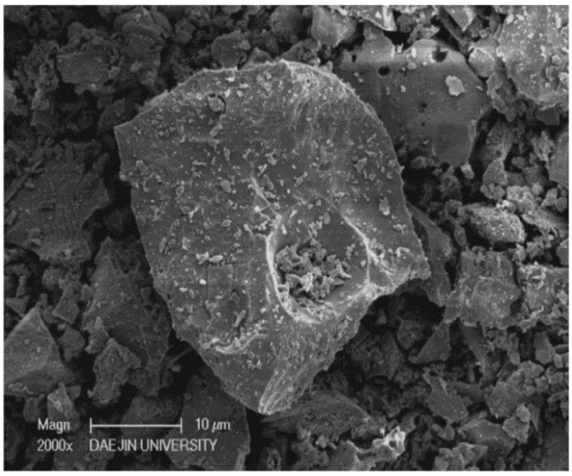

Fig. 4. 2 hrs ground wet bottom ash (Type 2) (× 2,000).

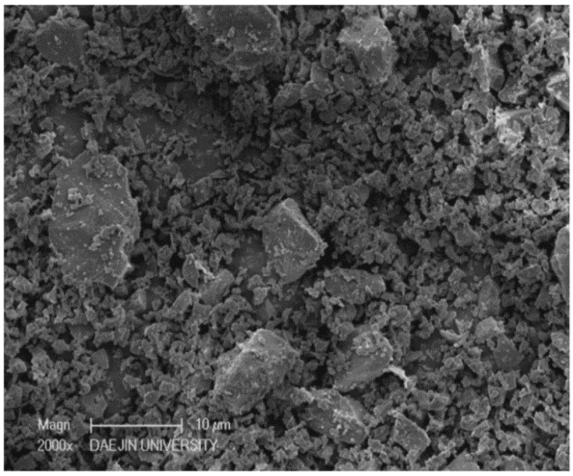

Fig. 5. 8 hrs ground bottom ash (Type 1) (× 2,000).

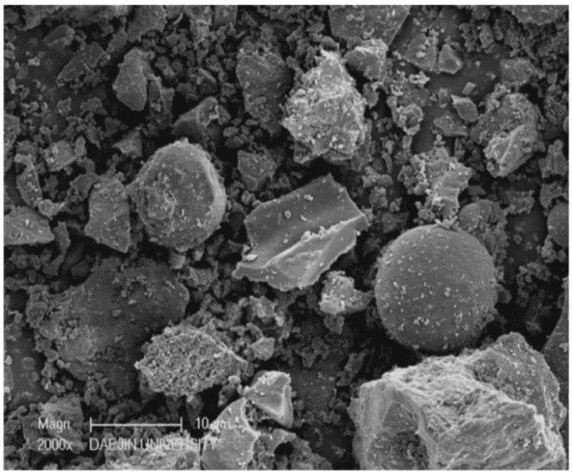

Fig. 6. 8 hrs ground wet bottom ash (Type 2) (× 2,000).

Test specimens were prepared using un-ground bottom ash, the finely ground bottom ashes, and fly ash as cement replacement. The flow and setting time were measured in a flash state, and the strength properties, porosities, and microstructures depending on the age were analyzed in order to examine the usability of bottom ash as a cement replacement.

Tables 1-3 present the physicochemical compositions of the cement, fly ash, and bottom ash used in this study.

Table 6. Test mortar mix.

Type		S/B	W/B (%)	Weight ratio/Grinding time (h)			
				Cement	Fly ash	Bottom ash (Type 1)	Bottom ash (Type 2)
Cement Mortar	PL	2.45	48.5	100	–	–	–
Fly ash Mortar	FA			75	25	–	–
Bottom ash (Type 1) Mortar	DBAP				–	25	–
	DBA1				–	25/1	–
	DBA2				–	25/2	–
	DBA3				–	25/4	–
	DBA6				–	25/8	–
Bottom ash (Type 2) Mortar	WBAP				–	–	25
	WBA3				–	–	25/1
	WBA5				–	–	25/2
	WBA6				–	–	25/4
	WBA9				–	–	25/8

(ex: DBA1 = mortar containing dry bottom ash particles with fineness 500-1499 cm^2/g after 1 h ball mill grinding.
WBA3 = mortar containing wet bottom ash particles with fineness 2500-3499 cm^2/g after 1 h ball mill grinding).

The bottom ash was subdivided into dry bottom ash (Type 1), discharged during dry processing, and wet bottom ash (Type 2), discharged during wet processing. Table 4 presents the physical properties of the river sand from the Jumunjin beach that was used as aggregate in the preparation of the mortar.

Both types of bottom ash were ground in a ball mill, because fine particles were considered better suited to use as filler than raw-state particles. The grinding times were set to 1, 2, 4, and 8 hrs. Figs. 1-6 show the scanning electron microscope (SEM) images of the dry and wet types of bottom ash before and after grinding. As shown in Figs. 1 and 2, the dry bottom ash emits carbon dioxide while melting, forming closed or open pores of various sizes. The wet bottom ash forms slurry-like aggregates by quenching with water. In addition, open pores with complicated structures are observed, as well as spherical particles identified as fly ash. As seen in Figs. 3-6, the pores are not visibly prominent on the smooth surfaces of the post-grinding bottom ash particles. The effect of grinding is also verified by the decreasing particle size and increasing number of particles proportional to the grinding time.

Prior to ball milling, the samples of bottom ash powder were passed through a sieve with a mesh size of 150 μm. After grinding for 1, 2, 4, and 8 hrs, the fineness and particle size of each sample were measured in compliance with ASTM C 204 [7] and ASTM E 1458 [8], respectively. The measurement results are presented in Table 5. As shown, the wet bottom ash samples exhibit larger specific surface areas than the dry bottom ash samples, presumably because the particle surfaces were softened by the water used to cool the bottom ash discharged from the boiler; the increased surface softness increased the grinding efficiency of the powder. Furthermore, as the grinding time is increased, the number of large particles (≥ 100 μm) decreases, gradually changing to fine particles (≤ 10 μm). This result is consistent with that of the coal-grinding experiment conducted by Heywood [9].

The mortar specimens were fabricated by replacing 25% of each of the selected binders with the specimen powders. All mortar mix ratios are listed in Table 6. The setting time and flow were measured in the unhardened state. Water absorption, porosity, and compressive strength were measured in the hardened specimens, and the micropore structure and hydration products were observed through microstructural analysis.

Setting time was measured in compliance with ASTM C 191 [10] to estimate the setting properties of the paste containing finely ground bottom ash.

Flow was measured in compliance with ASTM C 109 [11] to estimate the consistency of the martar containing finely ground bottom ash.

Water absorption and porosity were experimentally measured in compliance with ASTM C 642 [12] to estimate the relative density and hardening behavior of each specimen by identifying the physical properties related to moisture or foreign body penetration in the pores within the mortar. The weight changes were measured in indoor conditions after submerging the specimen in water until the interior of the specimen was saturated. The minimum temperature and relative humidity were maintained at 21-23 °C and 50%, and the water absorption and porosity were calculated with Eqs. (1) and (2), respectively.

$$WA(\%) = \left(\frac{W_2 - W_1}{W_1}\right) \times 100 \quad (1)$$

$$P(\%) = \left(\frac{W_2 - W_1}{W_2 - W_3}\right) \times 100 \quad (2)$$

where W_1, W_2, and W_3 are the sample weights in the states of full hardness, saturated surface hardness, and

submerged surface hardness, respectively.

Micropore-size distribution of the mortar containing the finely ground bottom ash was analyzed in compliance with ASTM D 4284 [13] using mercury intrusion porosimetry. Mortar specimens at Day 91 with unground and 8-hrs ground bottom ash (DBA6 and WBA9, respectively) were used for analysis. The pore diameters were measured within the range of 3 μm to 300 μm.

Compressive strength of the mortar specimens (40 mm 40 mm 40 mm) containing finely ground bottom ash as binder was measured in compliance with KS L 5105 [14] (Test Methods for Compressive Strength of Hydraulic Cement Mortars). In addition, the compressive strength was measured after 1, 3, 7, 28, 56, and 91 days of water curing at 20 ± 2 °C after being removed from the mold.

Microstructural analysis was performed on the hardened cement paste specimens containing finely ground bottom ash using X-ray diffraction (XRD), scanning electron microscopy (SEM), and energy-dispersive spectroscopy (EDS) in order to investigate the hydration behavior of the finely ground bottom ash. Similar to the method for mortar mixing, the cement paste specimens were fabricated by replacing 25% of the cement with finely ground bottom ash and fly ash, respectively. XRD analysis was performed to determine the reaction products within the paste. The measurement conditions for the XRD analysis were Cu Kα (Ni, filter) at 40 kV and 30 mA, 3 °/min scanning speed, full scale 140 cps, and 2θ = 5-60. For SEM observation and imaging, a Philips XL30 ESEM apparatus was used; EDS analysis was concurrently performed using a dispersive spectroscopy analyzer in order to determine the constituent elements of the specimen.

Results and Discussion

The setting times of the mortar mixes selected above were measured to determine the setting properties of the mortars containing finely ground bottom ash. The measured values are presented in Figs. 7 and 8. As shown, the mortar mixes containing unground bottom ash (DBAP, WBAP) exhibit the most delay in the initial and final setting times. Specifically, the initial and final setting times of the mortar containing finely ground dry bottom ash (DBA1-6) are delayed by 35-62 and 19-47 min, respectively, relative to the reference mortar (PL). The same times for the mortar containing finely ground wet bottom ash (WBA1-9) are 78-108 and 45-67 min. This phenomenon of delayed setting time is attributable to the insufficiency of the cement volume for early hydration because of the partial replacement with bottom ash. Slightly more rapid setting is observed as the grinding fineness of bottom ash is increased, suggesting that higher grinding fineness increases the viscosity of bottom ash, interfering with

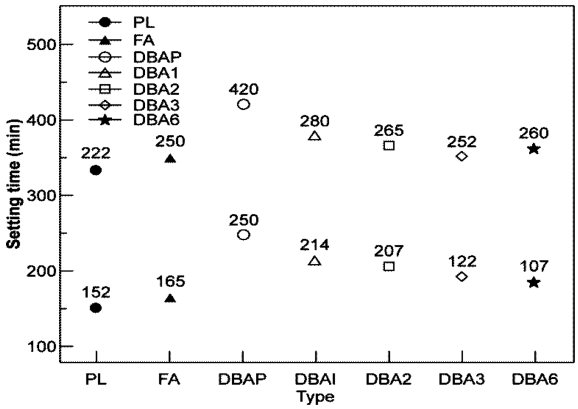

Fig. 7. Setting time (bottom ash mortar Type 1).Fig. 8. Setting time (bottom ash mortar Type 2).

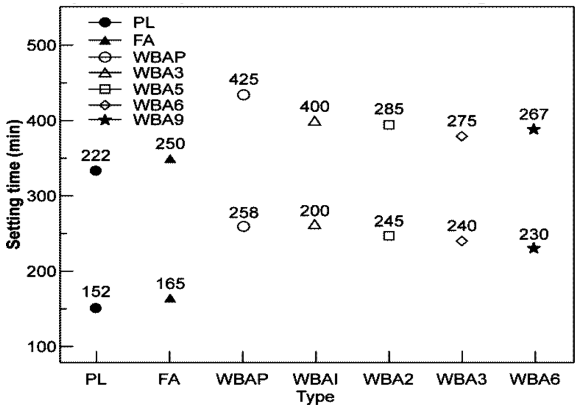

Fig. 8. Setting time (bottom ash mortar Type 2).

Vicat needle penetration and thus slightly decreasing the setting time. This explains the longer delays in the setting times of finely ground wet bottom ash compared to those of the dry type: wet bottom ash has higher fineness than dry bottom ash.

Flow testing was performed in compliance with KS L 5105 (Test Method for Compressive Strength of Hydraulic Cement Mortars). Table 7 presents the measurement values on the mortar flow table.

The mortar shapes of DBAP and WBAP undergo gradual deformation while falling from the flow table in the 25 repetitions of the experiments, causing difficulties in measuring the diameter. This deformation is presumably a result of the decreased flow caused by the high water absorption of bottom ash. The flow values of the mortars containing finely ground bottom ash tend to increase slightly with increases in the grinding fineness. To a small extent, this improved the properties of the bottom ash with high water absorption by converting porous structures of entangled particles to micro-fineness single particles in grinding.

Table 8 and Figs. 9-12 present the water absorption and porosity test results of the cement mortars produced using finely ground bottom ash. As shown, the water absorption and porosity of finely ground bottom ash tend to decrease as the curing age and

Table 7. Mortar flow.

Type	Flow (mm)	Type	Flow (mm)
PL	133	FA	120
DBAP	112	WBAP	110
DBA1	117	WBA3	112
DBA2	125	WBA5	121
DBA3	130	WBA6	129
DBA6	129	WBA9	128

Table 8. Water absorption and porosity of mortar specimens.

Type	Water absorption(%)			Porosity (%)		
	Day 7	Day 28	Day 91	Day 7	Day 28	Day 91
PL	3.36	2.12	1.06	7.33	4.46	2.28
FA	4.88	2.99	0.99	10.80	6.22	2.14
DBAP	7.14	6.28	5.87	15.00	12.43	11.66
DBA1	3.88	2.97	2.08	8.85	6.28	4.48
DBA2	3.78	2.44	1.47	8.86	5.16	3.18
DBA3	3.54	2.19	1.05	8.22	4.67	2.30
DBA6	4.29	2.17	0.83	9.76	4.59	1.81
WBAP	6.82	5.64	5.13	14.97	11.85	10.83
WBA3	4.51	3.39	2.31	10.41	7.08	4.96
WBA5	4.14	2.37	1.37	9.61	5.07	3.00
WBA6	4.22	2.35	1.00	9.96	4.99	2.19
WBA9	4.06	2.42	0.87	9.43	5.15	1.92

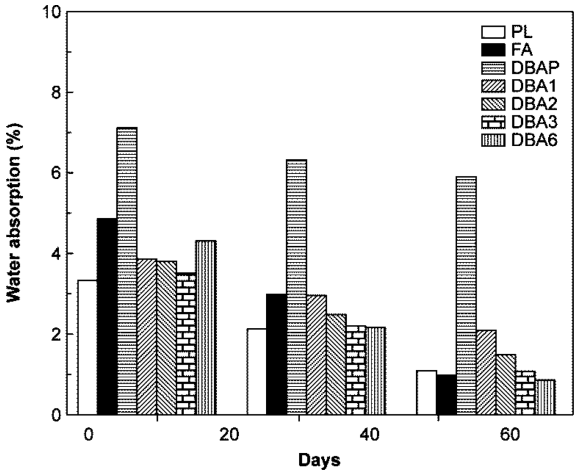

Fig. 9. Water absorption(bottom ash mortar Type 1).

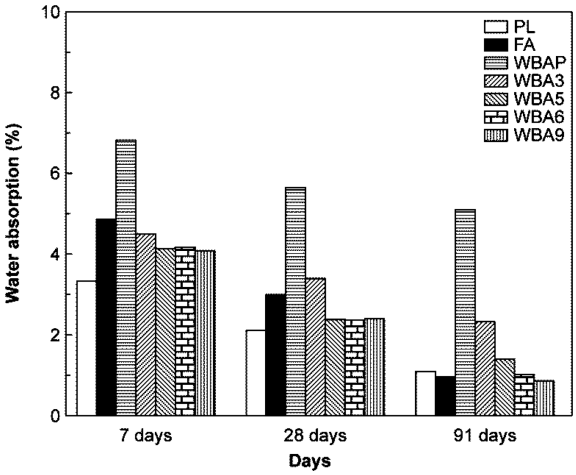

Fig. 10. Water absorption (bottom ash mortar Type 2).

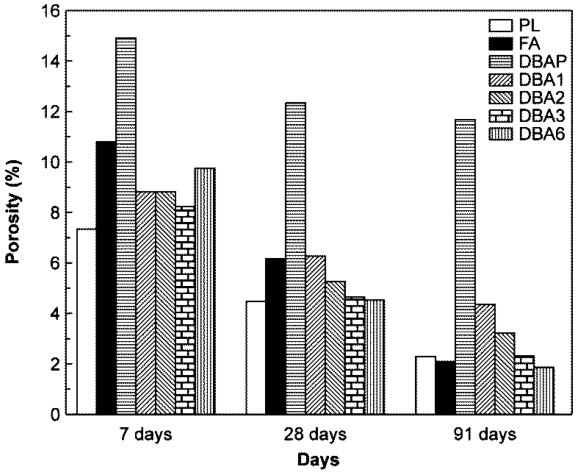

Fig. 11. Porosity (bottom ash mortar Type 1).

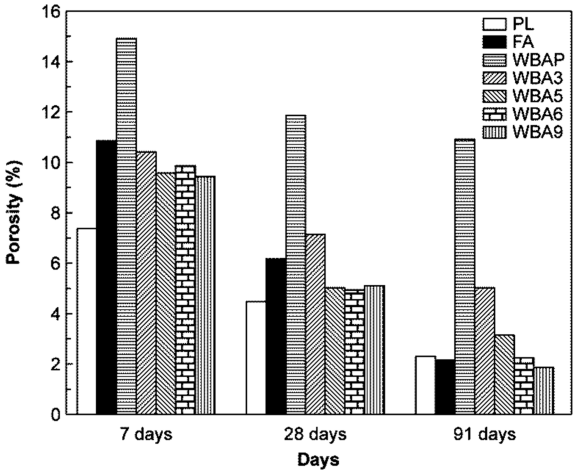

Fig. 12. Porosity (bottom ash mortar Type 2).

grinding fineness are increased. In particular, dry bottom ash with fineness $\geq 2{,}500\ cm^2/g$ (DBA3) and wet dry bottom ash with fineness $\geq 5{,}500\ cm^2/g$ (WBA6) demonstrate excellent reduction efficiency as the curing age is increased, similar to that of mortars containing fly ash. This is associated with the grinding fineness and pozzolanic reactivity of ground bottom ash; higher specific surface areas of the ground bottom ash correlate to stronger pozzolanic reactions, leading to decreased porosity by filling pores with the reaction products of the pozzolanic reactions.

The micropore structures of the Day 91 pastes containing finely ground and unground bottom ash were measured using mercury intrusion porosimetry. Figs. 13 and 14 present the measurement results. As shown, the paste containing unground bottom ash has more pores of 0.1-100 μm compared to the pastes

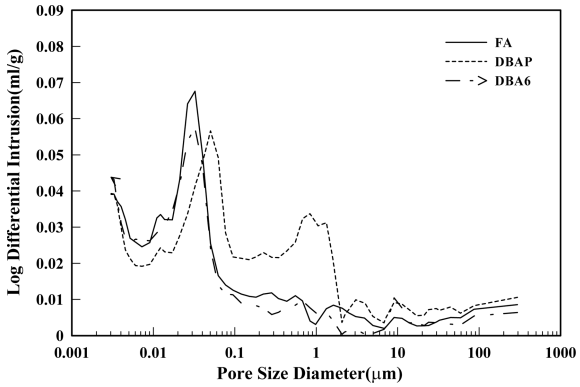

Fig. 13. Changes in micropore structure of the paste containing finely ground dry bottom ash.

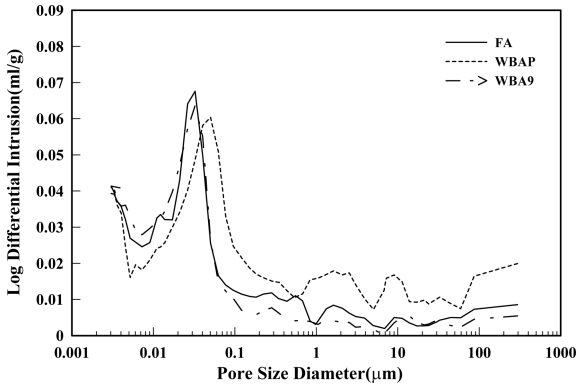

Fig. 14. Changes in micropore structure of the paste containing finely ground wet bottom ash.

containing fly ash; in the micropore size range of ≤ 0.1 μm, more and larger pores are distributed compared to those in the mortar containing fly ash. In contrast, pastes containing more finely ground bottom ash, e.g. DBA6 and WBA9, show micropore-size distributions similar to that of the paste containing fly ash. This is attributed to the effect of the pozzolanic reactions filling micropores with the reaction products, in the same manner as it affected water absorption and porosity.

Figs. 15 and 16 present the compressive strength measurement results of the mortar containing finely ground bottom ash from Day 1 through Day 91. As shown, the mortar shows increased strength as the curing age increases. In contrast, only negligible changes are observed in the compressive strength for a mortar containing unground bottom ash, presumably because of the lack of pozzolanic reactions. This allows the assumption that unprocessed bottom ash is unsuitable as concrete binder material. For mortars containing ground dry bottom ash, DBA3 and DBA6 exhibit strengths similar to that of PL in early ages, especially at curing ages ≥ Day 28. Similar results are observed for wet bottom ash (WBA6 and WBA9).

These results can be ascribed to the formation of an inorganic oxide coating around the particle surfaces of the bottom ash during ash generation. This coating, left

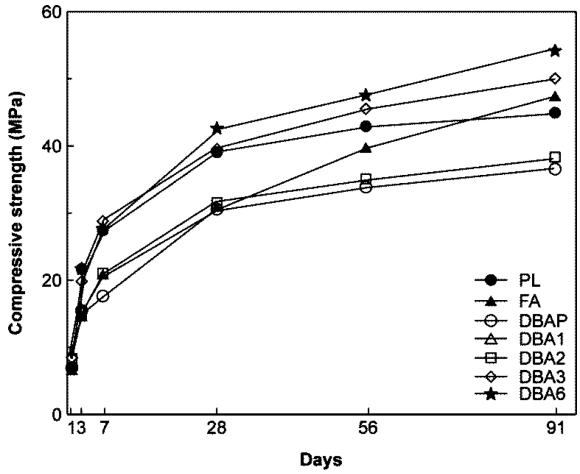

Fig. 15. Compressive strength(bottom ash mortar Type 1).

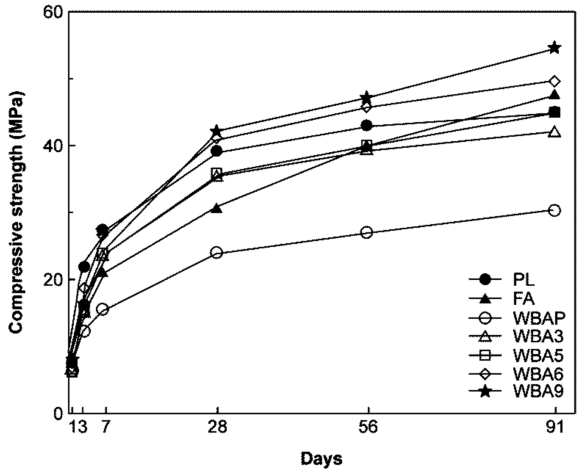

Fig. 16. Compressive strength(bottom ash mortar Type 2).

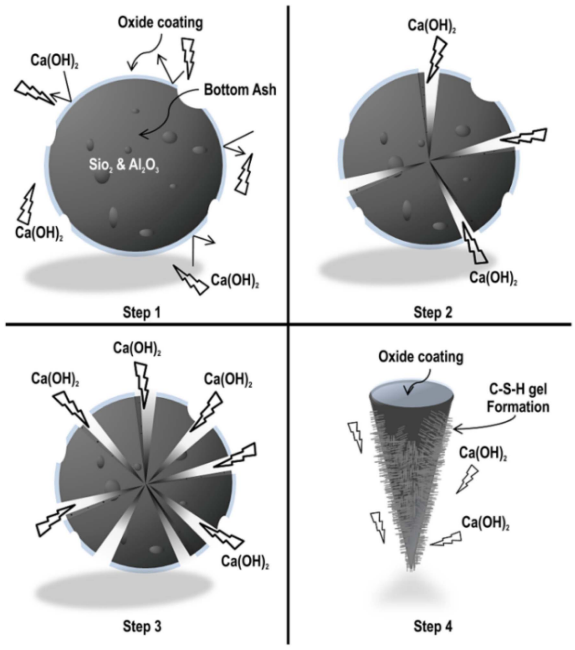

Fig. 17. Schematic of the pozzolanic reaction of finely ground bottom ash.

as a layer on the surface, interferes with chemical reactions. Grinding bottom ash thus destroys the oxide coating on the particle surfaces, whereby the reactive substances inside ($SiO_2 + Al_2O_3 + Fe_2O_3 + CaO$) can undergo pozzolanic reaction by reacting with $Ca(OH)_2$, thus generating C-S-H gel. Fig. 17 illustrates the mechanism of the grinding-induced increase in pozzolanic reactivity, assuming that the bottom ash particles have a spherical shape.

Furthermore, wet bottom ash shows a level of strength enhancement similar to that of dry bottom ash, despite the higher fineness. This can be attributed to the higher content of unburned carbon in the wet bottom ash, which suppresses the formation of pozzolanic reaction products compared to dry bottom ash.

From the physical properties of the cements using ground bottom ash, the following conclusions may be drawn. First, wet bottom ash has a lower specific reactivity than dry bottom ash because it has a much higher unburned carbon content. Second, higher grinding fineness corresponds to higher pozzolanic

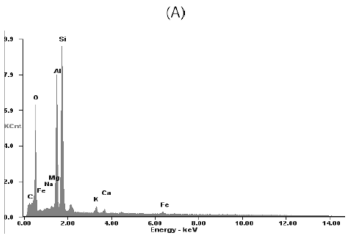

Element	Wt(%)	At(%)
C	12.26	19.70
O	40.38	48.71
Na	00.45	00.38
Mg	01.09	00.86
Al	01.98	01.42
Si	39.00	26.80
Ca	03.33	01.61
Fe	01.50	00.52

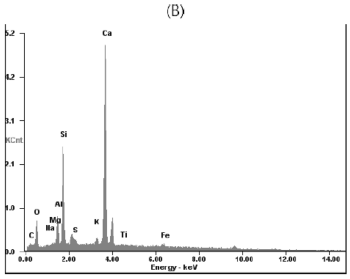

Element	Wt(%)	At(%)
C	07.67	14.02
O	33.60	46.13
Na	00.41	00.39
Mg	00.86	00.78
Al	02.94	02.40
Si	28.20	22.06
S	01.10	00.75
K	00.85	00.48
Ca	21.99	12.05
Fe	02.37	00.93

Fig. 18. Region-dependent EDS analysis results for a fly ash-added paste, corresponding to regions A and B in Fig. 19.

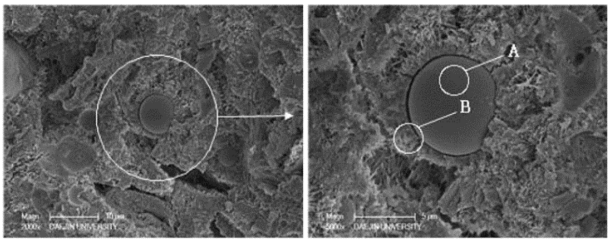

Fig. 19. SEM image of the paste containing fly ash (by Day 28).

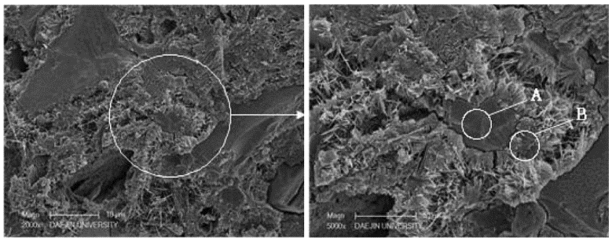

Fig. 20. SEM images of the cement paste containing bottom ash (Type 1) (Day 28).

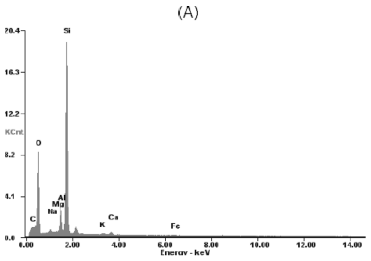

Element	Wt(%)	At(%)
C	11.55	19.07
O	35.69	44.21
Na	00.80	00.69
Mg	00.11	00.09
Al	05.80	04.26
Si	42.91	30.28
K	00.61	00.31
Ca	01.42	00.70
Fe	01.11	00.39

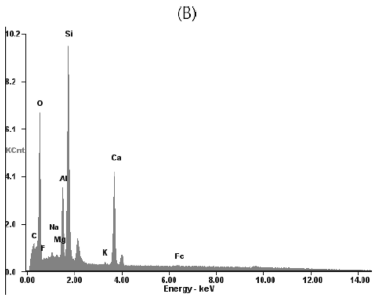

Element	Wt(%)	At(%)
C	09.09	15.79
O	38.24	49.89
F	00.12	00.13
Na	00.74	00.67
Mg	00.30	00.26
Al	07.15	05.53
Si	21.81	16.21
K	00.46	00.24
Ca	20.52	10.68
Fe	01.57	00.59

Fig. 21. Region-dependent EDS analysis results in a bottom ash-added cement paste (Type 1), from locations A and B in Fig. 20.

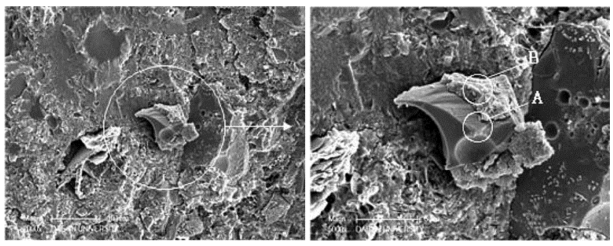

Fig. 22. SEM image of the cement paste containing bottom ash (Type 2) (Day 28)

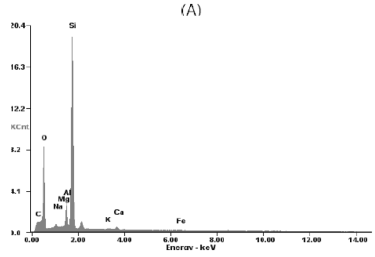

Element	Wt(%)	At(%)
C	10.80	18.08
O	37.07	46.59
Na	00.66	00.58
Mg	00.42	00.35
Al	08.16	06.08
Si	33.04	23.66
K	03.79	01.95
Ca	03.65	01.83
Tl	00.31	00.13

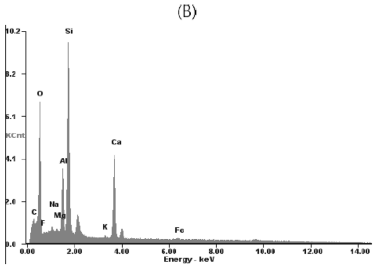

Element	Wt(%)	At(%)
C	10.33	17.66
O	38.91	49.93
Na	00.57	00.51
Mg	00.49	00.41
Al	07.20	05.48
Si	20.78	15.19
K	02.05	01.07
Ca	17.19	08.81
Tl	00.37	00.16
Fe	02.12	00.78

Fig. 23. Region-dependent EDS analysis results in a bottom ash-added cement paste (Type 2) from regions A and B in Fig. 22.

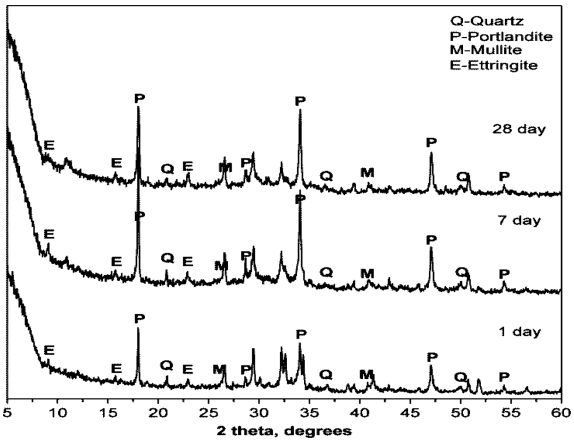

Fig. 24. XRD analysis results of the fly ash-added cement paste by age.

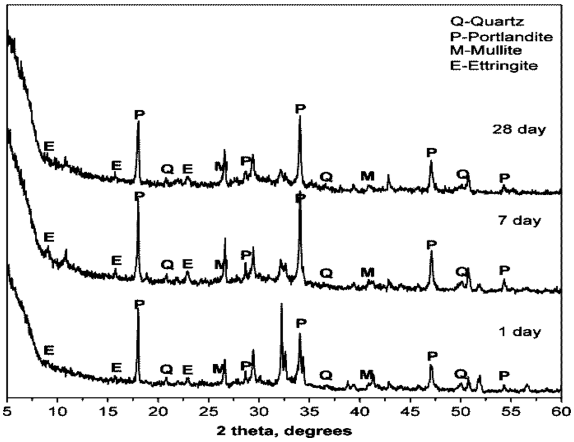

Fig. 25. XRD analysis results of the dry bottom ash-added cement paste by age.

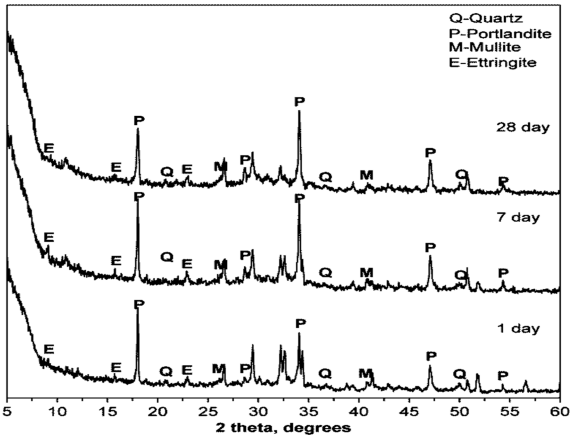

Fig. 26. XRD analysis results of the wet bottom ash-added cement paste by age.

reactivity; the dry bottom ash, with lower fineness, shows higher reactivity than the wet bottom ash. Third, both dry and wet bottom ash can be applied as cement binder, showing reactivity rates similar to that of fly ash at the fineness levels of $\geq$ 3,500 cm^2/g and $\geq$ 5,500 cm^2/g, respectively.

In this study, the products from the reactions of $Ca(OH)_2$ generated in the cement and the SiO_2 and Al_2O_3 constituting the bottom ash were confirmed using SEM imaging, EDS analysis, and XRD analysis. SEM was used to capture images of the regions expected to contain reaction products. After dividing the SEM regions into those not involved in reaction (A) and those with hydration-induced reaction products (B), EDS analysis was performed. Representative analysis results involving both fly ash and finely ground bottom ash are presented in Figs. 18-25.

Figs. 18 and 19 present images of the fly ash particles, in which layers of hydration products were observed on the surfaces. EDS-based composition analyses at points A and B, as illustrated in Figs. 18 and 19, confirm that the fly ash particle contains large amounts of SiO_2 and AlO_3 in A, whereas low-content Si and high-content Ca are observed in B, which is confirmed as a CSH gel hydration product.

Figs. 20-23 show the reaction products on the particle surfaces, as confirmed by the SEM imaging of the microstructures of the pastes containing finely ground dry and wet bottom ash, as well as the subsequent EDS analysis results. The EDS analyses confirm that A is a reaction product with SiO_2 and AlO_3 as main components, while B is a CSH-gel layer, judging from the increased calcium content.

Figs. 24-26 present the results of XRD analysis of the cement pastes containing fly ash and finely ground bottom ash. As shown, the peak values of the pastes containing finely ground bottom ash is similar to those of the pastes containing fly ash, allowing the assumption that the finely ground bottom ash undergoes hydration and pozzolanic reactions in a manner similar to the case of fly ash.

Summary and Conclusions

In this study, the physical properties and pozzolanic reactivity of finely ground bottom ash were investigated to assess the recycling potential of bottom ash, a waste product of thermal power plants, focusing on its usability as a cement replacement. The properties of bottom ash, finely ground using a rotary ball mill, were examined and compared to those of other fillers, using cement pastes and mortars containing varieties of bottom ash and fly ash. The experiments showed that bottom ash, when finely ground, has good potential for use as cement replacement; the porosity and pozzolanic reactivity can be improved by milling to levels approaching those of fly ash. It appears plausible to use bottom ash as a cementitious material; additional studies on the improvement of unburned coal contents or the durability of hardened cement using finely ground bottom ash may increase this plausibility. The following list summarizes the conclusions drawn from the results of this study.

1. By examining the setting time and pore properties

of the hardened cement specimens containing finely ground bottom ash, it was found that setting was delayed compared to that in the mortar specimens using cement only; the mix ratio should be reduced to obtain a certain consistency. Analyses of the micropore structures using mercury intrusion porosimetry and testing of the porosity and water absorption revealed that the pozzolanic reactions became more intense as the fineness of the finely ground bottom ash increased, and the interior structure of the mortar became denser.

2. The compressive strength of the mortar specimens was increased in proportion to the fineness of the bottom ash, showing strengths even higher than that of mortar with fly ash replacement. Furthermore, the dry bottom ash demonstrated higher performance in strength than wet bottom ash of the same fineness, presumably because the wet bottom ash has a lower level of reactive materials and a higher level of unburned coal carbon.

3. By analyzing the cement pastes containing the fly ash using SEM imaging, EDS analysis, and XRD analysis, gel layers attributed to reaction products were found on particle surfaces. Similar reaction products were confirmed in the specimens containing finely ground bottom ash, permitting the conclusion that pozzolanic reactions similar to those of fly ash can be expected of finely ground bottom ash.

Acknowledgements

This work was supported by the Development of the technology to improve the durability of marine structures using classification of coal ash of the Korea Institute of Energy Technology Evaluation and Planning (KETEP), granted financial resource from the Ministry of Trade, Industry & Energy, Republic of Korea (No. 20131020102300).

References

1. I.B. Topçu, T. Bilir, ACI Mater. J. 107 (2007) 48-56.
2. I. Yüksel, A. Genç, ACI Mater. J. 104 (2010) 397-403.
3. M. Singh, R. Siddique, ACI Mater. J. 112 (2015) 693-703.
4. N. Ghafoori, J. Buchole, ACI Mater. J. 94 (1997) 90-101.
5. İ. Kula, Y. Erdoğan, A. Olgun, O.M. Kalfa, V. Sevinç, Cem. Concr. Res. 31 (2001) 491-494.
6. M. Cheriaf, J. Cavalcante Rocha, J. Péra, Cem. Concr. Res. 29 (1999) 1387-1391.
7. ASTM C204-16, Standard test methods for fineness of hydraulic cement by air-permeability apparatus, ASTM International, West Conshohocken, PA, 2007, DOI: 10.1520/C0204-16.
8. ASTM E1458-12, Standard test method for calibration verification of laser diffraction particle sizing instruments using photomask reticles, ASTM International, West Conshohocken, PA, 2012, DOI: 10.1520/E1458-12.
9. H.C. Heywood, Imp. Coll. Eng. Soc. (1950) 6-26.
10. ASTM C191-13, Standard test methods for time of setting of hydraulic cement by Vicat needle, ASTM International, West Conshohocken, PA, 2013, DOI: 10.1520/C0191.
11. ASTM C109 / C109M-16a, Standard test methods for compressive strength of hydraulic cement mortars (using 2-in. or [50-mm] cube specimens), ASTM International, West Conshohocken, PA, 2016, DOI: 10.1520/C0109_C0109M-16A.
12. ASTM C642-13, Standard test method for density, absorption, and voids in hardened concrete, ASTM International, West Conshohocken, PA, 2013, DOI: 10.1520/C0642-13.
13. ASTM D4284-12, Standard test method for determining pore volume distribution of catalysts and catalyst carriers by mercury intrusion porosimetry, West Conshohocken, PA, 2012, DOI: 10.1520/D4284-12.
14. KS L 5105, Testing method for compressive strength of hydraulic cement mortars, Korea Standard, 2012.